Accepted Manuscript published as ERC-21-0179.R1. Accepted for publication: 16-Jul-2021

Whole Genome Sequencing of Single Circulating Tumor Cells from Neuroendocrine Neoplasms

Alexa Childs[1], Christopher D. Steele[1], Clare Vesely[1], Francesca M. Rizzo[1], Leah Ensell[1], Helen Lowe[1], Pawan Dhami[1], Heli Vaikkinen[1], Tu Vinh Luong[2], Lucia Conde[1], Javier Herrero[1], Martyn Caplin[3], Christos Toumpanakis[3], Christina Thirlwell[1,4], John A. Hartley[1], Nischalan Pillay[5,6], Tim Meyer[1,4]

[1]UCL Cancer Institute, University College London, London WC1E 6DD, UK

[2]Department of Histopathology, Royal Free London NHS Foundation Trust, London NW3 2QG, UK

[3]Department of Gastroenterology, Royal Free London NHS Foundation Trust, London NW3 2QG, UK

[4]Department of Oncology, Royal Free London NHS Foundation Trust, London NW3 2QG, UK

Research Department of Pathology, Cancer Institute, University College London, London WC1E 6BT, UK

[6]Department of Cellular and Molecular Pathology, Royal National Orthopaedic Hospital NHS Trust, Stanmore, Middlesex HA7 4LP, UK

Corresponding author: Professor Tim Meyer, UCL Cancer Institute, University College London. 72 Huntley Street, London WC1E 6DD, email; t.meyer@ucl.ac.uk

Tel; +44 207 679 6731.

Running title: WGS of single circulating tumor cells from NEN

Keywords: Neuroendocrine tumors, circulating tumor cells, single cell, copy number variation, whole genome sequencing

Word Count: 4998

Abstract

Single-cell profiling of circulating tumor cells (CTCs) as part of a minimally invasive liquid biopsy presents an opportunity to characterize and monitor tumor heterogeneity and evolution in individual patients. In this study, we aimed to compare single-cell copy number variation (CNV) data with tissue, and define the degree of intra- and inter-patient genomic heterogeneity. We performed next generation sequencing (NGS) whole genome CNV analysis of 125 single CTCs derived from seven patients with neuroendocrine neoplasms (NEN) alongside matched white blood cells (WBC), formalin fixed paraffin embedded (FFPE) and fresh frozen (FF) samples. CTC CNV profiling demonstrated recurrent chromosomal alterations in previously reported NEN copy number hotspots, including the prognostically relevant loss of chromosome 18. Unsupervised hierarchical clustering revealed CTCs with distinct clonal lineages as well as significant intra- and inter-patient genomic heterogeneity, including subclonal alterations not detectable by bulk analysis and previously unreported in NEN. Notably, we also demonstrate the presence of genomically distinct CTCs according to the enrichment strategy utilized (EpCAM-dependent versus size-based). This work has significant implications for the identification of therapeutic targets, tracking of evolutionary change and the implementation of CTC-biomarkers in cancer.

Background

The molecular characterization of tumors has advanced our understanding of the major somatic driver mutations and informed the development of targeted therapies, which have transformed outcomes in selected patient populations (Vogel

Accepted Manuscript published as ERC-21-0179.R1. Accepted for publication: 16-Jul-2021

et al., 2002, Sharma et al., 2007, Sosman et al., 2012). Whilst tissue biopsy remains central to diagnostic work-up, it is invasive, limited by the overall percentage of tumor cells and subject to heterogeneity exhibited in primary and metastatic tumors (Gerlinger et al., 2012, Walter et al., 2018, Navin et al., 2010). Furthermore, bulk genomic analysis cannot provide resolution at the single-cell level, which is required to fully define the extent of tumor heterogeneity.

Technological advances in whole genome amplification (WGA) and next generation sequencing (NGS) methods now permit genomic analysis at the single-cell level and are uniquely placed to unravel complex clonal structures and track tumor evolution over time. Furthermore, characterization of single circulating tumor cells (CTCs) as part of a minimally invasive “liquid biopsy” provides an opportunity to explore tumor biology and identify therapeutic targets.

The first clinical applications of CTCs focused on enumeration using the EpCAM-dependent CellSearch® platform, which has been shown to be both prognostic and predictive across a wide range of epithelial malignancies(Cristofanilli et al., 2004, Cohen et al., 2008, de Bono et al., 2008, Krebs et al., 2011, Poveda et al., 2011), including neuroendocrine neoplasms(Khan et al., 2013, Khan et al., 2016, Khan et al., 2011, Mandair et al., 2021). More recently, molecular analysis of single CTCs has been used to identify predictive biomarkers, such as the T790M resistance allele in NSCLC (Maheswaran et al., 2008). In SCLC, a pretreatment CTC-based biomarker has been shown to predict sensitivity to first line chemotherapy (Carter et al., 2017).

Neuroendocrine neoplasms (NEN) represent a heterogeneous disease entity with diverse histology, clinical features and prognosis (Dasari et al., 2017). They are characterized by a low mutational burden(Banck et al., 2013), but recurrent patterns of copy number variation (CNV) have been observed (Capurso et al., 2012, Cunningham et al., 2011, Kulke et al., 2008). CNVs affect a greater portion of the cancer genome than any other somatic genetic alteration (Heitzer et al., 2016) and CNV burden is prognostic for cancer-free and overall survival in multiple tumor types (Hieronymus et al., 2018) including NEN, where aneuploidy can be used to define distinct molecular subgroups of prognostic relevance (Karpathakis et al., 2016).

In this study, we perform CNV analysis of single NEN CTCs, aiming to define the extent of genomic heterogeneity both within and between patients, and to compare single-cell CTC data with bulk tissue analysis. CTC enrichment in NEN patients has to date been confined to EpCAM-dependent methodologies, which may fail to capture the full diversity of CTCs seen in this disease(Gorges et al., 2012). Here, we utilize both the EpCAM-based CellSearch® and epitope-independent Parsortix® systems in order to interrogate the full diversity of cells at the CNV level and investigate whether single cell CTCs may differ at a genomic level, according to EpCAM expression.

Methods

 Accepted Manuscript published as ERC-21-0179.R1. Accepted for publication: 16-Jul-2021

Patients

NEN patients were recruited at the Royal Free Hospital, London, between September 2014 and February 2018. The study was approved by the Local Ethics Committee (NRES Committee London – Bromley, IRAS ref 13/LO/0376) and all participants were required to provide written informed consent. Eligible patients had a histologically confirmed diagnosis of metastatic NEN in the absence of any other active malignancy. Tumors were graded according to the European Neuroendocrine Tumor Society (ENETS) guidelines(Bosman et al., 2010).

CTC enrichment using **CellSearch®**

Peripheral blood samples (7.5mls) were collected into CellSave tubes (Veridex LLC) stored at room temperature, and processed within 96 hours using the Celltracks® Autoprep® and Analyzer II® platform for the semi-automated staining, enrichment and enumeration of CTCs as previously described(Cristofanilli et al., 2005, Riethdorf et al., 2007). CTCs were defined as cells with a DAPI positive nucleus and positive EpCAM and cytokeratin expression in the absence of CD45 staining. All evaluations regarding enumeration of CTCs were made by two independent operators without knowledge of patient pathology. Enriched samples were re-suspended, aspirated from the CellSearch® cartridge and stored at -20°C in 50% glycerol.

CTC enrichment using Parsortix®

Blood was collected in Streck tubes (10ml) and incubated for 24-48 hours prior to size-based enrichment with the Parsortix® platform (ANGLE) using software protocols provided by the manufacturer. Following enrichment, samples were harvested in a total volume of 1.2mL of HBS by applying a reverse flow to the separation cassette. Enriched samples were resuspended in 200µl of autoMACS® Running Buffer and fixed and stained for further processing on a sterile Transwell polycarbonate membrane insert placed within a 50ml Falcon tube. BSA 3% (200µl) was pipetted to entirely cover its surface for a 10minute incubation. The 50ml tube was centrifuged at 500g for 2 minutes to elute the BSA solution from the filter prior to transferring the enriched patient sample onto the insert surface. 100µl of a 10% CD45 staining solution (10µl anti CD45-APC [Miltenyi Biotec] and 90µl of Running Buffer) and 100µl of a 10% CK staining solution solution (10µl anti CK-PE [Abcam] and 90µl Inside Perm [Miltenyi Biotec]) were used to sequentially stain samples for CD45 and cytokeratin prior to staining for nuclear content using 100µl of a 0.001mg/ml solution of Hoechst 33342 (Sigma Aldrich). After washing with SB115 buffer, the cell suspension was transferred into a sterile 1.5ml tube prior to volume reduction and loading into the DEPArray™ cartridge.

Cell Isolation from FFPE

FFPE tissue sections of 40-60µm thickness were dissociated into single cell suspensions and stained as previously described(Bolognesi et al., 2016). To enable visualization and identification of cells using the DEPArray™, cytokeratin and

 Accepted Manuscript published as ERC-21-0179.R1. Accepted for publication: 16-Jul-2021

vimentin were used as tumor and stromal cell markers respectively. Cell suspensions were stained with anti-cytokeratin MNF116 (IgG1) (DAKO), anti-cytokeratin AE1/AE3 (IgG1) (Millipore-Chemicon) and anti-Vimentin 3B4 (IgG2A) (DAKO).

Dissociated FFPE samples were subjected to a DNA quality control assay using the DEPArray™ FFPE QC kit (Silicon Biosystems). Each sample was given a QC score between 0-1 based on a qPCR-based assay. Samples with a sufficiently high DNA quality as determined by a QC score ≥0.4 according to manufacturer's guidelines were processed on the DEPArray™ platform for retrieval of single tumor cells.

Cell Isolation from fresh tissue

Fresh tissue samples were collected in RPMI 1640 medium (Gibco) and processed within 3 hours of collection. The tumor sample was placed in 1ml of dissociation solution (240µl collagenase, 150µl DNAse and 13.85ml of RPMI media) and processed in a gentleMacs™ dissociater for one cycle, followed by two consecutive 30 minute incubations at 37°C. Single cell suspensions were created using a 50µl cell strainer and centrifuged and re-suspended in 5ml of RPMI prior to re-suspending in 1ml of freezing medium (10% DMSO in FBS) for storage at -80°C. Samples were fixed with 2% paraformaldehyde (Fluka) for 20 minutes at room temperature prior to staining for cytokeratin, vimentin and DAPI performed as per FFPE samples.

DEPArray™ Sorting and Recovery

Both CellSearch® and Parsortix enriched samples were imaged and sorted using the DEPArray™ system (Silicon Biosystems) as per manufacturer's instructions(Abonnenc et al., 2013). Image–based selection was used to identify and recover individual cells

of interest as either single-cells or pools of cells, based on their morphological features, DNA content and fluorescence labelling; CTCs (CK-PE^{+}/CD45-APC^{-}/DAPI^{+}) and WBC (CK-PE^{-}/CD45-APC^{+}/DAPI^{+}).

For analysis of FFPE samples with the DEPArray™, between 5000 to 10000 stained cells were loaded into the cartridge and cell sorting executed according to DEPArray™ User's Manual rev 1.1_sw 2.1.1. The Cytokeratin+ Vimentin- tumor cell population and Cytokeratin-Vimentin+ stromal cell population were gated separately to evaluate morphology and staining characteristics prior to selecting cells for recovery.

Whole genome amplification of single-cell DNA and quality-control assay

WGA was performed on all recovered single-cells using the Ampli1™ WGA kit version 02 (Silicon Biosystems) as per manufacturer's instructions to generate a 50µl WGA product. For single cells derived from blood (CTCs and WBC) and fresh tissue (tumor and stromal cells), the quality of the WGA product was determined using the Ampli1™ QC Kit (Silicon Biosystems). A genomic integrity index (GII) was allocated for each sample, scored from 0-4. Only single-cells with sufficiently good quality DNA as determined by a GII≥2 were selected for downstream analysis.

Nucleic acid extraction

For bulk sequencing, DNA was extracted from 5 -10 sections of 10µm thickness from three FFPE blocks using the DNAstorm FFPE DNA Isolation Kit (CELLDATA) following manufacturers instructions. DNA was eluted into 75µl of nuclease free water and

Accepted Manuscript published as ERC-21-0179.R1. Accepted for publication: 16-Jul-2021

concentrations measured using the NanoDrop-1000 Spectrophotometer (NanoDrop) and Qubit 2.0 Flurormeter (Invitrogen). Haematoxylin and eosin-stained sections were evaluated to ensure >80% purity of tumor specimens prior to processing.

LowPass Whole Genome Sequencing and Bioinformatics

Ampli1™ LowPass kit for Illumina (Menarini Silicon Biosystems) was used for preparing low-pass Whole Genome Sequencing (WGS) libraries from single cells. For high-throughput processing, the manufacturer's procedure was implemented in a fully automated workflow on a STARlet Liquid Handling Robot (Hamilton®). Ampli1™ LowPass libraries were normalized and sequenced by HiSeq 2500 instrument using 150 SR rapid-run mode. The obtained FASTQ files were aligned to the hg19 human reference sequence using Burrows-Wheeler Aligner version 0.7.12 (BWA). Copy-number alterations in the data were identified using Control-FREEC software (version 11.0).

For bulk analysis of FFPE samples, genomic DNA was quantified using Qubit 3 fluorometer with dsDNA BR kit according to manufacturer's instructions. One microgram of genomic DNA was used to prepare whole genome sequencing libraries using Nonacus Cell 3 Target: Library Preparation kit. Library preparation was done according to manufacturer's instructions. Enzymatic fragmentation was performed at 32°C for 14 minutes to obtain library fragments with an average size of 250bp followed by ligation of UMI Adapters on both ends of the 5'-phosphorylated / 3'-dA-tailed DNA fragments. Libraries were purified using Target Pure NGS clean-up beads and minimal PCR amplification was carried out using 4 cycles of amplification.

198 Libraries were quantified using Qubit 3 fluorometer with dsDNA BR kit and run on an
199 Agilent Bioanalyzer DNA 1000 chip according to manufacturer's instructions. Average
200 library fragment length was determined from the bioanalyzer trace. Library molar
201 concentration was determined based on the average fragment size and the Qubit
202 concentration. All libraries were normalised to 10 nM working concentration and
203 pooled. The dual-indexed library pool was sequenced on Illumina Nextseq 500/550
204 platform to generate paired end reads. The Nonacus Cell 3 Target: Library
205 preparation protocol adds unique molecular identifiers (UMIs) to the sequencing
206 libraries which were sequenced by additional 9 cycles of sequencing added on to the
207 i7 index read.

208 Bulk sequencing data was processed with the nextflow Sarek v2.3.FIX1 pipeline
209 (https://github.com/UCL-BLIC/Sarek_v2.3.FIX1) following GATK best practices.
210 Specifically, reads were aligned against hg38 with BWA v0.7.17, duplicated reads
211 were marked and reads were recalibrated with GATK v4.1.1.0. CNV profiles were
212 obtained by running Control-FREEC v11.5 with WGS recommended parameters.

213 **Statistics**

214 All statistical analyzes were performed in R. Pairwise Manhattan distances were
215 calculated for all samples, using only copy number bins that were not NA for each
216 pair. Hierarchical clustering of copy number profiles using these distances was
217 performed with Ward's minimum variance method.

 Accepted Manuscript published as ERC-21-0179.R1. Accepted for publication: 16-Jul-2021

When comparing bulk and CTC copy number profiles, the mean copy number across CTC copy number bins that overlapped a bulk bin was taken. Any bulk bin without an overlapping CTC bin was not given a copy number designation.

t-distributed stochastic neighbour embedding (TSNE) analysis was performed using the R package Rtsne, using only the genomic bins that were non-missing for all samples analyzed, with a perplexity of 30.

Correlations between copy number profiles were calculated with respect to a base copy number of 2, as described in Zhang et al 2017(Gao et al., 2017):

$$\rho_{mn} = \frac{\sum_i (Cm_i - 2)(Cn_i - 2)}{\sqrt{\sum_j (Cm_j - 2)^2 \sum_k (Cn_k - 2)^2}}$$

Where ρ_{mn} is the correlation between samples m and n, while Cm_i is the copy number for sample *m* at bin *i*.

To account for differences in ploidy, correlation were also calculated with respect to the average copy number across all bins for each sample:

$$\rho_{mn} = \frac{\sum_i (Cm_i - P_m)(Cn_i - P_n)}{\sqrt{\sum_j (Cm_j - P_m)^2 \sum_k (Cn_k - P_n)^2}}$$

where P_m is the mean copy number for sample *m* across all bins.

Metrics chosen to investigate copy number dynamics within a sample were the proportion of genome altered (number of CN!=2 bins divided by the total number of bins) and Shannon's diversity index, $-\sum_i p_i ln\, p_i$, where p_i is the proportion of copy number bins with copy number state *i* i.e. CN=2. Tests for statistical differences

238 between distributions for these metrics were performed using the Kolgomorov-
239 Smirnov test.

240 Copy number gains and losses were defined in relation to ploidy. Gains were defined
241 as log2(CN/ploidy)>0.9, while losses were defined as log2(CN/ploidy)<-0.9. The
242 proportion of cells with a loss at a given genomic bin was used as a metric for a
243 single patient. When combining multiple patients the mean proportion of cells
244 across all patients considered was used. A threshold for statistically significant
245 recurrent gain or loss was determined by bootstrapping the original copy number
246 data; for each patient copy number states were sampled with replacement from
247 every copy number state seen in the original data for that patient, this was
248 performed for the same number of cells as were originally profiled for that patient.
249 Gains and losses were defined as previously, and the proportion of simulated cells
250 with a gain/loss at each genomic bin was calculated. This was repeated 1000 times
251 per patient, and the threshold for determining recurrent gains/losses was set as
252 99.9^{th} percentile value across all genomic bins for gains or losses separately. For a
253 threshold where multiple patients are being considered, the same bootstrapping was
254 performed for each patient, but the threshold was determined as the 99.9^{th}
255 percentile of the mean proportion of cells with gain/loss across the patients being
256 evaluated.

257 **Results**

 Accepted Manuscript published as ERC-21-0179.R1. Accepted for publication: 16-Jul-2021

Patient characteristics and sample collection

Seven NEN patients were included with primary tumor sites comprising the small intestine (SINET) (n=4), pancreas (n=1), gastro-oesophageal junction (GOJ) (n=1) and kidney (n=1). All patients had peripheral blood samples taken for CTC enrichment using the EpCAM-dependent CellSearch® platform and three patients had concomitant samples enriched using the size-based Parsortix® device (Figure 1). Blood samples were taken from new patients at time of first presentation to our clinic (patients 1, 3, 5, 6) or at time of disease progression prior to commencing systemic therapy (patients 2, 4, 7). Matched WBC were analyzed as negative controls. A total of 7 tissue samples (6 FFPE, 1 FF) from six patients were analysed. Of the seven samples, four were primary tumor samples (3 small intestine, 1 GOJ) and three were metastatic sites (2 liver, 1 brain). One patient (patient 1) had no available tissue for analysis. The clinical and treatment characteristics as well as the samples analyzed per patient are summarized in Table 1.

CTC sequencing

In total, 125 single CTCs were isolated from seven patients and successfully subjected to whole genome amplification (WGA), quality-control PCR and low pass whole genome sequencing (LPWGS). Single CTCs displayed high quality metrics, with only 3.5% failing to pass the quality checks for single-cell CNV. As a control, 17 single WBC (CD45 positive cells) were isolated and subjected to the same procedures. CD45 positive cells showed balanced copy number profiles (Supplementary Figure 1) whereas CTCs showed multiple gains and losses (Figures 2 and 3), confirming the aberrant nature of these tumor cells and the uniformity of single-cell WGA with the

Ampli1™ kit. The sensitivity and specificity of CTC identification and recovery by the DEPArray™ was assessed across all single cells subjected to LPWGS. Cells with CNV profiles demonstrating an overabundance of substantial chromosomal gains and losses were considered CTCs, whilst cells demonstrating flat profiles were classified as WBC(Ferrarini et al., 2018, Mangano et al., 2019). Using CNV profiles as the ultimate classifier of cell status, DEPArray™ selection had a positive predictive value of 95% and negative predictive value of 100% (P<0.0001).

Single tumor cells derived from FFPE surgical specimens/biopsies were also subjected to the same procedures as CTCs. DNA quality of single cell suspensions was assessed using the Ampli1™ QC Kit (Silicon Biosystems) prior to cell sorting. Four of the seven samples had QC values ≥0.4 indicating a sufficient DNA quality for single-cell CNV analysis and 8-10 single cells from each sample were processed for CNV analysis. The majority of single tumor cells had high derivative log ratio spread values in keeping with low library quality and only 15% of recovered single cells yielded sufficient quality results for CNV analysis.

CTC versus tumor tissue CNV profiles

For the three patients with sufficient matched FFPE tissue available for bulk analysis, whole-genome CNV profiles were compared between CTCs and bulk FFPE samples (Figure 2). The CNVs demonstrated in bulk tissue analysis were predominantly losses and these were also detectable in most CTCs. For example, in patient 2, losses in chromosomes 6, 9 and 18 are seen in bulk tissue and in 25, 80 and 65% of CTCs respectively, while patient 3, losses in chromosome 16 were observed in bulk tissue

 Accepted Manuscript published as ERC-21-0179.R1. Accepted for publication: 16-Jul-2021

and 100% of CTCs (Figure 2). The majority of these concordant genomic losses are located in regions of the genome previously described as altered in NENs, with loss of chromosome 9 and 18 reported in 20% and 60-78% of SINETS respectively. However, single CTC data demonstrated the presence of clones enriched in additional somatic copy number alterations not detectable at bulk level, including the presence of a subclone of cells with evidence of whole genome doubling, observed in patients 2 (10% of CTCs) and 4 (6%). These reproducible CNV patterns were not evident in bulk sequencing analysis, and only detectable due to the resolution afforded by single cell sequencing. Such subclonal copy number alterations were most pronounced in patient 4, where appreciable CNV gains or losses were only detectable at the single cell level and not in the bulk tissue.

In patient 3, single tumor cells derived from a fresh frozen (FF) liver biopsy exhibited identical copy number profiles as CTCs and unsupervised hierarchical clustering of CTC and tumor copy number profiles demonstrated clustering of these cells together.

CTC analysis reveals significant inter- and intrapatient heterogeneity

To fully explore inter- and intrapatient CNV heterogeneity in NEN patients, the full set of 125 single CTCs from seven patient samples were further interrogated (Figure 3). Copy number losses were seen more frequently than amplifications, however, whole genome doubling was detected in all CTCs derived from two patients (Patients 1 and 6). Despite the preponderance of losses, the CNV patterns of individual patients are dissimilar and this remains the case when considering only those

patients of small intestinal primary site (patients 1-4). These patient-specific patterns of CNV were confirmed using t-distributed stochastic neighbour embedding (TSNE; Figure 4), which demonstrated clear clustering of individual patients, with no segregation according to primary site. Conversely, all WBC clustered together regardless of patient of origin in keeping with their flat CNV profiles (Figure 4b).

Within individual patients there were observations of clonal CN alterations seen in 100% of CTCs, but also clear evidence of subclonal changes and of individual cells with unique CNV profiles indicative of divergent evolution (Figure 3). This intra-patient heterogeneity was only detectable at the single cell level. The degree of intra-patient heterogeneity varied according to patient, with patients 3 and 6 demonstrating the highest average pairwise correlation of CTC CNV profiles, and hence the most homogenous copy number landscape across CTCs (Supplementary Figure 2). However, the correlation of CNV profiles within patients remains higher than that observed between patients, underscoring the independent nature of CNV profiles originating in different patients, and the shared evolutionary history of CTCs, and thus CTC CNV profiles, within individual patients.

CNV profiles vary according to enrichment strategy

In patient 7, hierarchical clustering of CNV profiles demonstrated distinct clustering of CTCs enriched by the EpCAM-dependent CellSearch® as compared to the epitope-independent, size-based Parsortix® platform (Figure 3). This is also demonstrated in Figure 4 where Parsortix® and CellSearch® CTCs from patient 7 form largely separate groups. To investigate this further, we summarized single CTC profiles via two

 Accepted Manuscript published as ERC-21-0179.R1. Accepted for publication: 16-Jul-2021

metrics; the proportion of the genome that is aberrant (copy number other than 2), and copy number diversity as enumerated by Shannon's diversity index, and compared these metrics across cells according to the enrichment strategy utilized. There was a statistically significant difference in the distribution of both metrics between different enrichment strategies within patient 7 (Kolgomorov-Smirnov test, $p<0.01$, Figure 5A), where Parsortix® CTCs demonstrate a larger range in both metrics as compared to CellSearch® CTCs, indicating greater cell-to-cell variation. Interestingly, the difference seen in patient 7 were not found to be statistically significant across all patients (Figure 5B), indicating that these differences may vary on a patient-to-patient basis. This data suggests that restricting analysis of CTCs to only those that express EpCAM may exclude subsets of tumor cells that could be clinically relevant.

CTC Molecular Characterization

In order to evaluate the clinical application of CTC CNV profiling as a surrogate for tissue biopsy, we interrogated CTC CNV profiles for prognostic or actionable copy number changes described in the NEN literature. Evaluation of the frequency of copy number amplifications and deletions within CTC CNV profiles from SINET patients revealed recurrent losses of Chromosomes 9, 13q, 16q and 18 (Figure 6A). These have previously been described in SINETs supporting the technical reliability of our data and the potential use of CTCs as a tissue surrogate(Di Domenico et al., 2017, Karpathakis et al., 2016, Hashemi et al., 2013, Banck et al., 2013, Kulke et al., 2008). Of particular note is Chromosome 18, loss of which is the most frequently reported

genomic event in SINET, occurring in 60-78% of tumors, and is of prognostic relevance(Karpathakis et al., 2016). Previously unreported alterations, including loss of Chromosome 2p and 7q22 were also identified. Although not reported in SINET, allelic losses in Chromosome 2p are reported in colorectal, lung and endometrial malignancies. The tumor suppressor gene *CUX1* is located at Chromosome 7q22, knockdown of which causes increased PI3K signaling and AKT phosphorylation(Ramdzan and Nepveu, 2014). This may be relevant in this patient population as deregulation of the PI3K/Akt/mTOR pathway is well-established in NEN, supported by the clinical efficacy of the mTOR inhibitor everolimus(Yao et al., 2011, Pavel et al., 2011).

Whole chromosome and arm gains at Chromosome 4 have previously been described in SINET. We did not observe such large-scale gains, instead, we observed focal gains in the TEC gene on Chromosome 4p12, which encodes a protein belonging to the Tec family of non-receptor protein-tyrosine kinases involved in the T-lymphocyte activation pathway and implicated in myelodysplastic syndrome.

CTCs from patient 7 (renal NET) demonstrated recurrent chromosomal alterations of likely clinical significance. Loss of Chromosome 3p was observed in a high proportion of CTCs, and harbors several tumor suppressor genes including the VHL gene at 3p25. Loss of heterozygosity (LOH) of 3p has been reported in the limited renal NET sequencing data available and is also found in over 90% of clear cell renal carcinoma(Alimov et al., 2000, el-Naggar et al., 1995). Loss of Chromosomes 10q and 13q were also observed, the former of which encodes the tumor suppressor gene

 Accepted Manuscript published as ERC-21-0179.R1. Accepted for publication: 16-Jul-2021

391 PTEN and is of prognostic relevance in renal cell carcinoma(Velickovic et al., 2002).
392 Finally, as with SINET, Chromosome 16q loss was frequently identified across patient
393 7 CTCs. Deletion of 16q is demonstrated across multiple malignancies, and LOH has
394 been indicated as an early event in the development of breast and hepatocellular
395 cancer with possible prognostic implications(Hansen et al., 1998, Sakai et al., 1992).

396 **Discussion**

397 Copy number analysis of NEN CTCs confirmed a wide range of genomic aberrations
398 making them readily distinguishable from WBC. All cells classified as WBC using the
399 pre-determined DEPArray™ criteria demonstrated balanced copy number profiles,
400 confirming the specificity and reproducibility of these criteria and accuracy of
401 DEPArray™ sorting.

402

403 In this study we show for the first time that somatic CNVs of NEN CTCs mirror those
404 seen in FFPE tissue, validating these CTC enrichment and isolation technologies in
405 NEN and confirming their potential use as a surrogate for tissue biopsy. The clinical
406 applications of this finding have been demonstrated in other tumor types such as
407 NSCLC, where good concordance between ALK-rearranged CTCs and ALK-positive
408 tumor biopsies has been demonstrated(Pailler et al., 2013). This finding is
409 particularly relevant in tumor types where tissue biopsy is not readily available or as
410 in NEN, where the relatively good prognosis of patients with low grade disease
411 means surgical specimens or biopsies may have been taken several years previously
412 and therefore not be representative of the current genomic landscape of the disease

after multiple lines of systemic therapy. CTCs have the additional benefit of being non-invasive and therefore easily repeatable, thus allowing the monitoring of genomic change in real-time. Beyond this, serial CTC monitoring may also enable the detection of mechanisms of resistance(Pailler et al., 2015). Importantly, subclonal CNVs not discernible in bulk tissue analysis were detectable in single CTC samples thus allowing the identification of intra-patient genomic heterogeneity.

Unsupervised hierarchical clustering identified intrapatient genomic heterogeneity in NEN patients, with diverse single CTC CNV traces observed in some patients. The intrapatient CNV heterogeneity demonstrated in this study has also been observed in other tumor types such as prostate (Lambros et al., 2018, Dago et al., 2014) and colorectal(Heitzer et al., 2013) cancer. This is in contrast to lung adenocarcinoma, SCLC, breast and gastric cancer, where more homogeneous CNV have been observed in CTCs from individual patients(Heidary et al., 2014, Ni et al., 2013, Gao et al., 2017). Intrapatient heterogeneity is of clinical relevance as it may impact upon prognosis, response to treatment and biomarker development. High intratumoral heterogeneity in tissue samples has been associated with a worse overall survival across different tumor types(Mroz et al., 2013, Seol et al., 2012). This relationship has not yet been examined with regards to the genomic profiling of CTCs, but low phenotypic diversity of prostate cancer CTCs has been shown to correlate with improved OS in patients treated with androgen receptor signalling inhibitors (ARSI), whereas high heterogeneity was associated with increased risk of death on ARSI relative to taxanes. Considerable heterogeneity was also demonstrated in CNV patterns between patients. This appears to be cancer-type specific. Ni et al observed almost identical global CNV patterns in 5 different patients with lung

Accepted Manuscript published as ERC-21-0179.R1. Accepted for publication: 16-Jul-2021

adenocarcinoma with 78% of the gain and loss regions shared between any two patients(Ni et al., 2013) and similar findings have been reported in gastric cancer(Gao et al., 2017). However, increased inter-patient heterogeneity is seen in other tumor types, such as SCLC and breast cancer(Gao et al., 2017, Ni et al., 2013). The inter-patient heterogeneity in CNV profiles demonstrated in this study persists even when analysis is confined to those patients with small-intestinal primaries.

Epitope-dependent enrichment technologies such as the CellSearch® platform limit recovery of CTCs to an EpCAM-positive subpopulation. In this study we performed the first direct comparison of CTC CNV profiles using identical blood draws between the epitope-independent size-based Parsortix® and EpCAM-based CellSearch®. In patient 7, CTCs enriched using the CellSearch® platform demonstrate reproducible CNV with high inter-cell concordance. However, CTCs enriched using Parsortix® appear genomically distinct, lacking the conserved CNV demonstrated in CellSearch® CTCs and displaying a wider range of inter-cell heterogeneity. Different methods of enrichment may therefore impact on the results of single-cell genomic analysis and have implications for serial monitoring of CNV profiles. This finding is clinically significant as it may impact on biomarker development. For example, a CNV-based classifier of CTCs has been shown to predict chemosensitivity in SCLC patients(Carter et al., 2017). In that study, all CTCs were enriched using CellSearch® and the classifier was less effective in those patients demonstrating intra-patient heterogeneity. The data presented in our study suggests that the efficacy of CNV-based classifiers such as this may be affected by the form of enrichment used and could not be directly extrapolated to CTCs enriched using alternative technologies. Furthermore, it

suggests combining epitope-independent enrichment strategies with CellSearch® may allow sampling of a wider population of CTCs with greater potential to fully capture CTC diversity.

SINET are characterized by a low mutational burden, with the most frequent mutation occurring in the cell cycle regulator CDKN1B (cyclin-dependent kinase inhibitor 1B) in only 8% of tumors(Francis et al., 2013, Crona et al., 2015). In this study, we identify recurrent loss of Chromosome 18, the most common genomic event in SINET and predictive of PFS in SINET. Karpathakis et al have previously demonstrated that CNV analysis of SINET primary tissue can be used to divide patients into three molecular subtypes with significant impact on PFS(Karpathakis et al., 2016). We also demonstrate novel and potentially targetable alterations such as focal gains in Chromosome 4p12, which encodes the TEC gene(Yu and Smith, 2011). Further work is required to validate this finding in a larger cohort of patients.

Despite the novel findings reported, we acknowledge some limitations; namely the relatively low number of patients involved, as well as their heterogeneity in terms of grade and primary site. However, limiting analysis to a smaller patient cohort allowed assessment of multiple CTCs per patient in order to better characterize intra-patient heterogeneity, whilst the overall large number of single cells analysed allowed comparison with bulk tissue data and of cell enrichment techniques at the molecular level.

 Accepted Manuscript published as ERC-21-0179.R1. Accepted for publication: 16-Jul-2021

In conclusion, this is the first study to demonstrate that CNV analysis of single CTCs in NEN patients is feasible. We have demonstrated significant intra- and inter-patient genomic heterogeneity undetected by bulk tissue analysis. Additionally, we demonstrate for the first time, the presence of genomically distinct CTCs according to the enrichment strategy utilized, which has implications for the study of CTCs across all tumour types.

Conflict of interest: there is no conflict of interest that could be perceived as prejudicing the impartiality of the research reported

Funding: This work was supported by the CRUK & EPSRC Comprehensive Cancer Imaging Centre, European Neuroendocrine Tumor Society Fellowship, University College London (UCL) CRUK and NIHR Experimental Cancer Medicine Centre Grant No. C12125/A15576, MRC award MR/M009033/1 and the UCL Hospitals NIHR Biomedical Research Centre.

References

ABONNENC, M., MANARESI, N., BORGATTI, M., MEDORO, G., FABBRI, E., ROMANI, A., ALTOMARE, L., TARTAGNI, M., RIZZO, R., BARICORDI, O., et al. 2013. Programmable interactions of functionalized single bioparticles in a dielectrophoresis-based microarray chip. *Anal Chem,* 85**,** 8219-24.

ALIMOV, A., KOST-ALIMOVA, M., LIU, J., LI, C., BERGERHEIM, U., IMREH, S., KLEIN, G. & ZABAROVSKY, E. R. 2000. Combined LOH/CGH analysis proves the existence of interstitial 3p deletions in renal cell carcinoma. *Oncogene,* 19**,** 1392-9.

BANCK, M. S., KANWAR, R., KULKARNI, A. A., BOORA, G. K., METGE, F., KIPP, B. R., ZHANG, L., THORLAND, E. C., MINN, K. T., TENTU, R., et al. 2013. The genomic landscape of small intestine neuroendocrine tumors. *J Clin Invest,* 123**,** 2502-8.

BOLOGNESI, C., FORCATO, C., BUSON, G., FONTANA, F., MANGANO, C., DOFFINI, A., SERO, V., LANZELLOTTO, R., SIGNORINI, G., CALANCA, A., et al. 2016. Digital Sorting of Pure Cell Populations Enables Unambiguous Genetic Analysis of Heterogeneous Formalin-Fixed Paraffin-Embedded Tumors by Next Generation Sequencing. *Sci Rep,* 6**,** 20944.

BOSMAN, F. T., CARNEIRO, F., HRUBAN, R. H. & THEISE, N. D. 2010. *WHO Classification of Tumours*, IARC.

514 CAPURSO, G., FESTA, S., VALENTE, R., PICIUCCHI, M., PANZUTO, F., JENSEN, R. T. & DELLE
515 FAVE, G. 2012. Molecular pathology and genetics of pancreatic endocrine tumours. *J*
516 *Mol Endocrinol,* 49**,** R37-50.
517 CARTER, L., ROTHWELL, D. G., MESQUITA, B., SMOWTON, C., LEONG, H. S., FERNANDEZ-
518 GUTIERREZ, F., LI, Y., BURT, D. J., ANTONELLO, J., MORROW, C. J., et al. 2017.
519 Molecular analysis of circulating tumor cells identifies distinct copy-number profiles
520 in patients with chemosensitive and chemorefractory small-cell lung cancer. *Nat*
521 *Med,* 23**,** 114-119.
522 COHEN, S. J., PUNT, C. J., IANNOTTI, N., SAIDMAN, B. H., SABBATH, K. D., GABRAIL, N. Y.,
523 PICUS, J., MORSE, M., MITCHELL, E., MILLER, M. C., et al. 2008. Relationship of
524 circulating tumor cells to tumor response, progression-free survival, and overall
525 survival in patients with metastatic colorectal cancer. *J Clin Oncol,* 26**,** 3213-21.
526 CRISTOFANILLI, M., BUDD, G. T., ELLIS, M. J., STOPECK, A., MATERA, J., MILLER, M. C.,
527 REUBEN, J. M., DOYLE, G. V., ALLARD, W. J., TERSTAPPEN, L. W., et al. 2004.
528 Circulating tumor cells, disease progression, and survival in metastatic breast cancer.
529 *N Engl J Med,* 351**,** 781-91.
530 CRISTOFANILLI, M., HAYES, D. F., BUDD, G. T., ELLIS, M. J., STOPECK, A., REUBEN, J. M.,
531 DOYLE, G. V., MATERA, J., ALLARD, W. J., MILLER, M. C., et al. 2005. Circulating
532 tumor cells: a novel prognostic factor for newly diagnosed metastatic breast cancer.
533 *J Clin Oncol,* 23**,** 1420-30.
534 CRONA, J., GUSTAVSSON, T., NORLEN, O., EDFELDT, K., AKERSTROM, T., WESTIN, G.,
535 HELLMAN, P., BJORKLUND, P. & STALBERG, P. 2015. Somatic Mutations and Genetic
536 Heterogeneity at the CDKN1B Locus in Small Intestinal Neuroendocrine Tumors. *Ann*
537 *Surg Oncol,* 22 Suppl 3**,** S1428-35.
538 CUNNINGHAM, J. L., DIAZ DE STAHL, T., SJOBLOM, T., WESTIN, G., DUMANSKI, J. P. &
539 JANSON, E. T. 2011. Common pathogenetic mechanism involving human
540 chromosome 18 in familial and sporadic ileal carcinoid tumors. *Genes Chromosomes*
541 *Cancer,* 50**,** 82-94.
542 DAGO, A. E., STEPANSKY, A., CARLSSON, A., LUTTGEN, M., KENDALL, J., BASLAN, T.,
543 KOLATKAR, A., WIGLER, M., BETHEL, K., GROSS, M. E., et al. 2014. Rapid phenotypic
544 and genomic change in response to therapeutic pressure in prostate cancer inferred
545 by high content analysis of single circulating tumor cells. *PLoS One,* 9**,** e101777.
546 DASARI, A., SHEN, C., HALPERIN, D., ZHAO, B., ZHOU, S., XU, Y., SHIH, T. & YAO, J. C. 2017.
547 Trends in the Incidence, Prevalence, and Survival Outcomes in Patients With
548 Neuroendocrine Tumors in the United States. *JAMA Oncol,* 3**,** 1335-1342.
549 DE BONO, J. S., SCHER, H. I., MONTGOMERY, R. B., PARKER, C., MILLER, M. C., TISSING, H.,
550 DOYLE, G. V., TERSTAPPEN, L. W., PIENTA, K. J. & RAGHAVAN, D. 2008. Circulating
551 tumor cells predict survival benefit from treatment in metastatic castration-resistant
552 prostate cancer. *Clin Cancer Res,* 14**,** 6302-9.
553 DI DOMENICO, A., WIEDMER, T., MARINONI, I. & PERREN, A. 2017. Genetic and epigenetic
554 drivers of neuroendocrine tumours (NET). *Endocr Relat Cancer,* 24**,** R315-r334.
555 EL-NAGGAR, A. K., TRONCOSO, P. & ORDONEZ, N. G. 1995. Primary renal carcinoid tumor
556 with molecular abnormality characteristic of conventional renal cell neoplasms.
557 *Diagn Mol Pathol,* 4**,** 48-53.
558 FERRARINI, A., FORCATO, C., BUSON, G., TONONI, P., DEL MONACO, V., TERRACCIANO, M.,
559 BOLOGNESI, C., FONTANA, F., MEDORO, G., NEVES, R., et al. 2018. A streamlined
560 workflow for single-cells genome-wide copy-number profiling by low-pass
561 sequencing of LM-PCR whole-genome amplification products. *PLoS One,* 13**,**
562 e0193689.

 Accepted Manuscript published as ERC-21-0179.R1. Accepted for publication: 16-Jul-2021

563 FRANCIS, J. M., KIEZUN, A., RAMOS, A. H., SERRA, S., PEDAMALLU, C. S., QIAN, Z. R., BANCK,
564 M. S., KANWAR, R., KULKARNI, A. A., KARPATHAKIS, A., et al. 2013. Somatic mutation
565 of CDKN1B in small intestine neuroendocrine tumors. *Nat Genet,* 45**,** 1483-6.
566 GAO, Y., NI, X., GUO, H., SU, Z., BA, Y., TONG, Z., GUO, Z., YAO, X., CHEN, X., YIN, J., et al.
567 2017. Single-cell sequencing deciphers a convergent evolution of copy number
568 alterations from primary to circulating tumor cells. *Genome Res,* 27**,** 1312-1322.
569 GERLINGER, M., ROWAN, A. J., HORSWELL, S., MATH, M., LARKIN, J., ENDESFELDER, D.,
570 GRONROOS, E., MARTINEZ, P., MATTHEWS, N., STEWART, A., et al. 2012. Intratumor
571 heterogeneity and branched evolution revealed by multiregion sequencing. *N Engl J*
572 *Med,* 366**,** 883-892.
573 GORGES, T. M., TINHOFER, I., DROSCH, M., ROSE, L., ZOLLNER, T. M., KRAHN, T. & VON
574 AHSEN, O. 2012. Circulating tumour cells escape from EpCAM-based detection due
575 to epithelial-to-mesenchymal transition. *BMC Cancer,* 12**,** 178.
576 HANSEN, L. L., YILMAZ, M., OVERGAARD, J., ANDERSEN, J. & KRUSE, T. A. 1998. Allelic loss of
577 16q23.2-24.2 is an independent marker of good prognosis in primary breast cancer.
578 *Cancer Res,* 58**,** 2166-9.
579 HASHEMI, J., FOTOUHI, O., SULAIMAN, L., KJELLMAN, M., HOOG, A., ZEDENIUS, J. &
580 LARSSON, C. 2013. Copy number alterations in small intestinal neuroendocrine
581 tumors determined by array comparative genomic hybridization. *BMC Cancer,* 13**,**
582 505.
583 HEIDARY, M., AUER, M., ULZ, P., HEITZER, E., PETRU, E., GASCH, C., RIETHDORF, S.,
584 MAUERMANN, O., LAFER, I., PRISTAUZ, G., et al. 2014. The dynamic range of
585 circulating tumor DNA in metastatic breast cancer. *Breast Cancer Res,* 16**,** 421.
586 HEITZER, E., AUER, M., GASCH, C., PICHLER, M., ULZ, P., HOFFMANN, E. M., LAX, S.,
587 WALDISPUEHL-GEIGL, J., MAUERMANN, O., LACKNER, C., et al. 2013. Complex tumor
588 genomes inferred from single circulating tumor cells by array-CGH and next-
589 generation sequencing. *Cancer Res,* 73**,** 2965-75.
590 HEITZER, E., ULZ, P., GEIGL, J. B. & SPEICHER, M. R. 2016. Non-invasive detection of genome-
591 wide somatic copy number alterations by liquid biopsies. *Mol Oncol,* 10**,** 494-502.
592 HIERONYMUS, H., MURALI, R., TIN, A., YADAV, K., ABIDA, W., MOLLER, H., BERNEY, D.,
593 SCHER, H., CARVER, B., SCARDINO, P., et al. 2018. Tumor copy number alteration
594 burden is a pan-cancer prognostic factor associated with recurrence and death. *Elife,*
595 7.
596 KARPATHAKIS, A., DIBRA, H., PIPINIKAS, C., FEBER, A., MORRIS, T., FRANCIS, J., OUKRIF, D.,
597 MANDAIR, D., PERICLEOUS, M., MOHMADUVESH, M., et al. 2016. Prognostic Impact
598 of Novel Molecular Subtypes of Small Intestinal Neuroendocrine Tumor. *Clin Cancer*
599 *Res,* 22**,** 250-8.
600 KHAN, M. S., KIRKWOOD, A., TSIGANI, T., GARCIA-HERNANDEZ, J., HARTLEY, J. A., CAPLIN, M.
601 E. & MEYER, T. 2013. Circulating tumor cells as prognostic markers in
602 neuroendocrine tumors. *J Clin Oncol,* 31**,** 365-72.
603 KHAN, M. S., KIRKWOOD, A. A., TSIGANI, T., LOWE, H., GOLDSTEIN, R., HARTLEY, J. A.,
604 CAPLIN, M. E. & MEYER, T. 2016. Early Changes in Circulating Tumor Cells Are
605 Associated with Response and Survival Following Treatment of Metastatic
606 Neuroendocrine Neoplasms. *Clin Cancer Res,* 22**,** 79-85.
607 KHAN, M. S., TSIGANI, T., RASHID, M., RABOUHANS, J. S., YU, D., LUONG, T. V., CAPLIN, M. &
608 MEYER, T. 2011. Circulating tumor cells and EpCAM expression in neuroendocrine
609 tumors. *Clin Cancer Res,* 17**,** 337-45.
610 KREBS, M. G., SLOANE, R., PRIEST, L., LANCASHIRE, L., HOU, J. M., GREYSTOKE, A., WARD, T.
611 H., FERRALDESCHI, R., HUGHES, A., CLACK, G., et al. 2011. Evaluation and prognostic
612 significance of circulating tumor cells in patients with non-small-cell lung cancer. *J*
613 *Clin Oncol,* 29**,** 1556-63.

KULKE, M. H., FREED, E., CHIANG, D. Y., PHILIPS, J., ZAHRIEH, D., GLICKMAN, J. N. & SHIVDASANI, R. A. 2008. High-resolution analysis of genetic alterations in small bowel carcinoid tumors reveals areas of recurrent amplification and loss. *Genes Chromosomes Cancer,* 47**,** 591-603.

LAMBROS, M. B., SEED, G., SUMANASURIYA, S., GIL, V., CRESPO, M., FONTES, M., CHANDLER, R., MEHRA, N., FOWLER, G., EBBS, B., et al. 2018. Single-Cell Analyses of Prostate Cancer Liquid Biopsies Acquired by Apheresis. *Clin Cancer Res*.

MAHESWARAN, S., SEQUIST, L. V., NAGRATH, S., ULKUS, L., BRANNIGAN, B., COLLURA, C. V., INSERRA, E., DIEDERICHS, S., IAFRATE, A. J., BELL, D. W., et al. 2008. Detection of mutations in EGFR in circulating lung-cancer cells. *N Engl J Med,* 359**,** 366-77.

MANDAIR, D., KHAN, M. S., LOPES, A., FURTADO O'MAHONY, L., ENSELL, L., LOWE, H., HARTLEY, J. A., TOUMPANAKIS, C., CAPLIN, M. & MEYER, T. 2021. Prognostic Threshold for Circulating Tumor Cells in Patients With Pancreatic and Midgut Neuroendocrine Tumors. *J Clin Endocrinol Metab,* 106**,** 872-882.

MANGANO, C., FERRARINI, A., FORCATO, C., GARONZI, M., TONONI, P., LANZELLOTTO, R., RASPADORI, A., BOLOGNESI, C., BUSON, G., MEDORO, G., et al. 2019. Precise detection of genomic imbalances at single-cell resolution reveals intra-patient heterogeneity in Hodgkin's lymphoma. *Blood Cancer J,* 9**,** 92.

MROZ, E. A., TWARD, A. D., PICKERING, C. R., MYERS, J. N., FERRIS, R. L. & ROCCO, J. W. 2013. High intratumor genetic heterogeneity is related to worse outcome in patients with head and neck squamous cell carcinoma. *Cancer,* 119**,** 3034-42.

NAVIN, N., KRASNITZ, A., RODGERS, L., COOK, K., METH, J., KENDALL, J., RIGGS, M., EBERLING, Y., TROGE, J., GRUBOR, V., et al. 2010. Inferring tumor progression from genomic heterogeneity. *Genome Res,* 20**,** 68-80.

NI, X., ZHUO, M., SU, Z., DUAN, J., GAO, Y., WANG, Z., ZONG, C., BAI, H., CHAPMAN, A. R., ZHAO, J., et al. 2013. Reproducible copy number variation patterns among single circulating tumor cells of lung cancer patients. *Proc Natl Acad Sci U S A,* 110**,** 21083-8.

PAILLER, E., ADAM, J., BARTHELEMY, A., OULHEN, M., AUGER, N., VALENT, A., BORGET, I., PLANCHARD, D., TAYLOR, M., ANDRE, F., et al. 2013. Detection of circulating tumor cells harboring a unique ALK rearrangement in ALK-positive non-small-cell lung cancer. *J Clin Oncol,* 31**,** 2273-81.

PAILLER, E., AUGER, N., LINDSAY, C. R., VIELH, P., ISLAS-MORRIS-HERNANDEZ, A., BORGET, I., NGO-CAMUS, M., PLANCHARD, D., SORIA, J. C., BESSE, B., et al. 2015. High level of chromosomal instability in circulating tumor cells of ROS1-rearranged non-small-cell lung cancer. *Ann Oncol,* 26**,** 1408-15.

PAVEL, M. E., HAINSWORTH, J. D., BAUDIN, E., PEETERS, M., HORSCH, D., WINKLER, R. E., KLIMOVSKY, J., LEBWOHL, D., JEHL, V., WOLIN, E. M., et al. 2011. Everolimus plus octreotide long-acting repeatable for the treatment of advanced neuroendocrine tumours associated with carcinoid syndrome (RADIANT-2): a randomised, placebo-controlled, phase 3 study. *Lancet,* 378**,** 2005-2012.

POVEDA, A., KAYE, S. B., MCCORMACK, R., WANG, S., PAREKH, T., RICCI, D., LEBEDINSKY, C. A., TERCERO, J. C., ZINTL, P. & MONK, B. J. 2011. Circulating tumor cells predict progression free survival and overall survival in patients with relapsed/recurrent advanced ovarian cancer. *Gynecol Oncol,* 122**,** 567-72.

RAMDZAN, Z. M. & NEPVEU, A. 2014. CUX1, a haploinsufficient tumour suppressor gene overexpressed in advanced cancers. *Nat Rev Cancer,* 14**,** 673-82.

RIETHDORF, S., FRITSCHE, H., MULLER, V., RAU, T., SCHINDLBECK, C., RACK, B., JANNI, W., COITH, C., BECK, K., JANICKE, F., et al. 2007. Detection of circulating tumor cells in peripheral blood of patients with metastatic breast cancer: a validation study of the CellSearch system. *Clin Cancer Res,* 13**,** 920-8.

Accepted Manuscript published as ERC-21-0179.R1. Accepted for publication: 16-Jul-2021

665 SAKAI, K., NAGAHARA, H., ABE, K. & OBATA, H. 1992. Loss of heterozygosity on chromosome
666 16 in hepatocellular carcinoma. *J Gastroenterol Hepatol,* 7**,** 288-92.
667 SEOL, H., LEE, H. J., CHOI, Y., LEE, H. E., KIM, Y. J., KIM, J. H., KANG, E., KIM, S. W. & PARK, S.
668 Y. 2012. Intratumoral heterogeneity of HER2 gene amplification in breast cancer: its
669 clinicopathological significance. *Mod Pathol,* 25**,** 938-48.
670 SHARMA, S. V., BELL, D. W., SETTLEMAN, J. & HABER, D. A. 2007. Epidermal growth factor
671 receptor mutations in lung cancer. *Nat Rev Cancer,* 7**,** 169-81.
672 SOSMAN, J. A., KIM, K. B., SCHUCHTER, L., GONZALEZ, R., PAVLICK, A. C., WEBER, J. S.,
673 MCARTHUR, G. A., HUTSON, T. E., MOSCHOS, S. J., FLAHERTY, K. T., et al. 2012.
674 Survival in BRAF V600-mutant advanced melanoma treated with vemurafenib. *N*
675 *Engl J Med,* 366**,** 707-14.
676 VELICKOVIC, M., DELAHUNT, B., MCIVER, B. & GREBE, S. K. 2002. Intragenic PTEN/MMAC1
677 loss of heterozygosity in conventional (clear-cell) renal cell carcinoma is associated
678 with poor patient prognosis. *Mod Pathol,* 15**,** 479-85.
679 VOGEL, C. L., COBLEIGH, M. A., TRIPATHY, D., GUTHEIL, J. C., HARRIS, L. N., FEHRENBACHER,
680 L., SLAMON, D. J., MURPHY, M., NOVOTNY, W. F., BURCHMORE, M., et al. 2002.
681 Efficacy and safety of trastuzumab as a single agent in first-line treatment of HER2-
682 overexpressing metastatic breast cancer. *J Clin Oncol,* 20**,** 719-26.
683 WALTER, D., HARTER, P. N., BATTKE, F., WINKELMANN, R., SCHNEIDER, M., HOLZER, K.,
684 KOCH, C., BOJUNGA, J., ZEUZEM, S., HANSMANN, M. L., et al. 2018. Genetic
685 heterogeneity of primary lesion and metastasis in small intestine neuroendocrine
686 tumors. *Sci Rep,* 8**,** 3811.
687 YAO, J. C., SHAH, M. H., ITO, T., BOHAS, C. L., WOLIN, E. M., VAN CUTSEM, E., HOBDAY, T. J.,
688 OKUSAKA, T., CAPDEVILA, J., DE VRIES, E. G., et al. 2011. Everolimus for advanced
689 pancreatic neuroendocrine tumors. *N Engl J Med,* 364**,** 514-23.
690 YU, L. & SMITH, C. I. 2011. Tec family kinases. *FEBS J,* 278**,** 1969.

691 **Figure Legends:**

692 **Figure 1. Experimental design of the study.** Workflow used in the study to enrich for CTCs
693 and CNV profiling using Ampli1 WGA and LowPass kit for Illumina. Following enrichment
694 (EpCAM-dependent versus size-based platforms), single NEN CTCs and matched WBC are
695 selectively recovered in dynamically controlled dielectrophoretic cages using the DEPArray
696 Image-Assisted Digital Cell Sorter. CTC samples undergo WGA and QC prior to low-resolution
697 whole-genome sequencing for CNV profiling. Where surgical resection or biopsy specimens
698 are available, samples are processed for bulk LPWGS and single cell LPWGS as per CTCs.

699

700 **Figure 2. Comparison of low-resolution whole-genome copy number profiles for CTCs and**
701 **bulk tissue reveals reproduction of the majority of the CNV from the formalin fixed**
702 **paraffin embedded (FFPE) and fresh frozen (FF) tissue in CTC samples.** Unsupervised
703 hierarchical clustering heat map of each analyzed individual CTC and tissue sample based on
704 CNV from 3 SINET patients. Each patient is depicted with one color as shown on the
705 phenobar at the bottom of the heat map. Individual CTCs are categorized according to
706 enrichment method and tissue into bulk versus single cell FFPE (see key). Chromosomal CNV
707 are shown from top to bottom for each individual cell or sample; copy-number gains are
708 depicted in blue, losses in orange.

709

710 **Figure 3. Individual CTC CNV data depicting complex intrapatient and interpatient genomic**
711 **diversity**. Unsupervised hierarchical clustering heat map of all analysed CTCs based on CNV
712 across seven patients. Each patient is depicted with one color as shown on the phenobar at
713 the bottom of the heat map along with cell sorting method and primary NET site.

714

 Accepted Manuscript published as ERC-21-0179.R1. Accepted for publication: 16-Jul-2021

715 **Figure 4. Relationship between CTCs from all 7 NEN patients is revealed through TSNE**
716 **analysis.** (A) Single CTCs from all seven patients are visualised and can be identified by color
717 in the phenobar at the top of the figure. Cells are also depicted according to enrichment
718 strategy (see key). (B) TSNE of all analyzed CTCs and WBC.

719

720 **Figure 5. Distribution plot describing the impact of enrichment strategy in patient 7 (A)**
721 **and all patients (B) on the proportion of the genome that is aberrant and CNV diversity as**
722 **quantified by Shannon Index.** Each small line represents the described value for a single
723 CTC. Large bars represent mean values.

724

725 **Figure 6. Frequency of genomic amplifications and deletions across all CTCs.** Profiles
726 demonstrated for SINET patients (A) Patient 5; pancreatic NEN (B) Patient 6; GOJ NEN (C)
727 and patient 7; renal NEN (D).

728

729 **Supplementary Figure 1. Cluster analysis of copy number profiles for CD45 positive cells**
730 **reveals balanced copy number profiles.** Each patient is depicted with one color as shown on
731 the phenobar at the bottom of the heat map. Profiles are distinct from CTCs and in keeping
732 with WBC populations.

733

734 **Supplementary Figure 2. Average pairwise correlation for CNV profiles within (diagonal)**
735 **and between (off-diagonal) patients.** After adjusting for ploidy, there was low correlation
736 between individual patients. The degree of heterogeneity varied on a per patient basis, with
737 LPWGS demonstrating more homogenous CNV profiles and therefore lower intra-patient
738 heterogeneity in patients 3 and 6.

Patient ID	Sex	Age	Primary Site	Grade	Treatment	CellSearch CTCs	Parsortix CTCs	WBC	Fresh tissue single cells	FFPE single cells	FFPE bulk samples
1	M	74	Small intestine	2	na	4	na	4	na	na	na
2	F	45	Small intestine	3	PEN-221	15	5	na	na	2	Pituitary metastasis
3	F	69	Small intestine	2	na	7	8	na	8	na	Small bowel
4	M	65	Small intestine	1	SSA	18	na	na	na	na	Small bowel
5	M	47	Pancreas	2	na	12	na	4	na	na	na
6	M	64	GOJ	3	na	11	na	na	na	1	na
7	F	33	Renal	2	PEN-221	21	11	10	na	2	na

Table 1. Summary of clinical characteristics

M: male, F: female, na: not applicable, GOJ: Gastro-oesophageal junction, SSA: Somatostatin analogues, PEN-221: novel antibody-drug conjugate, FFPE: formalin fixed paraffin embedded. All tissue samples are FFPE unless specifically indicated otherwise.

Accepted Manuscript published as ERC-21-0179.R1. Accepted for publication: 16-Jul-2021

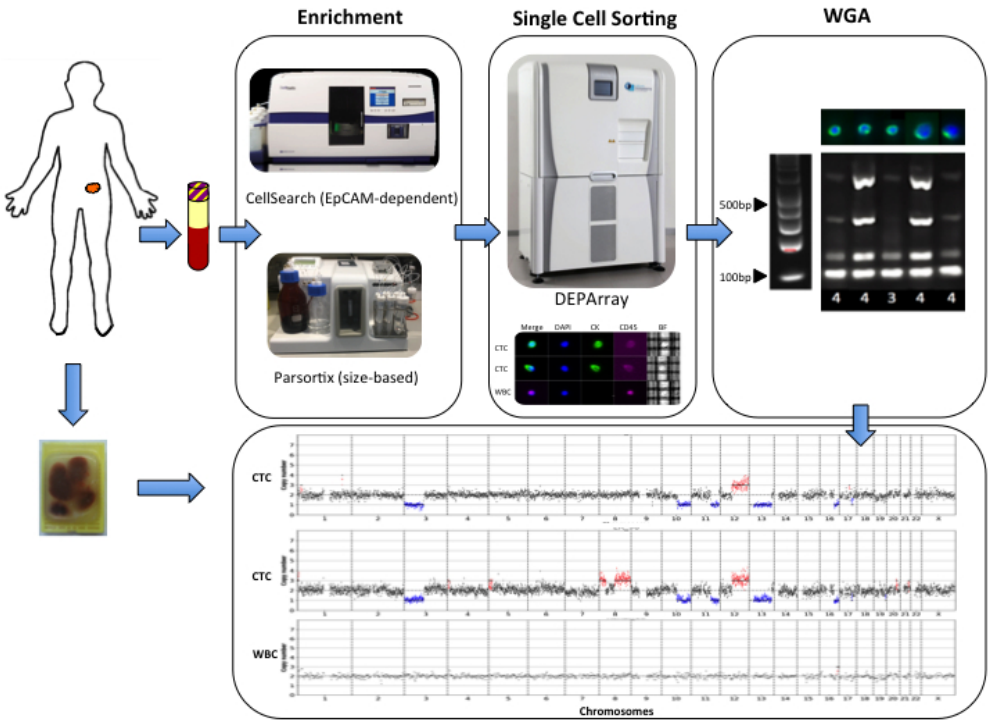

Figure 1. Experimental design of the study. Workflow used in the study to enrich for CTCs and CNV profiling using Ampli1 WGA and LowPass kit for Illumina. Following enrichment (EpCAM-dependent versus size-based platforms), single NEN CTCs and matched WBC are selectively recovered in dynamically controlled dielectrophoretic cages using the DEPArray Image-Assisted Digital Cell Sorter. CTC samples undergo WGA and QC prior to low-resolution whole-genome sequencing for CNV profiling. Where surgical resection or biopsy specimens are available, samples are processed for bulk LPWGS and single cell LPWGS as per CTCs.

254x190mm (72 x 72 DPI)

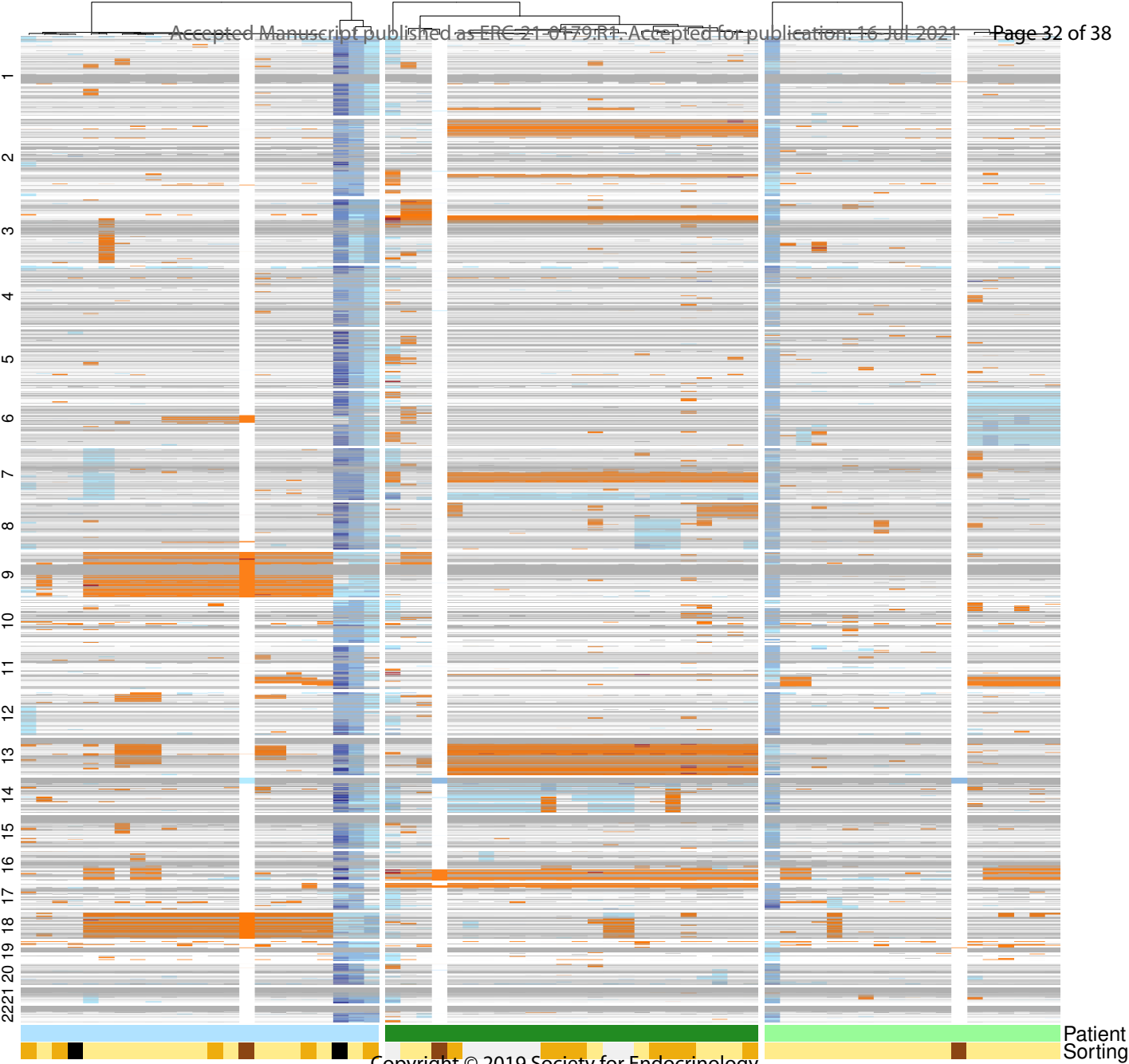

Accepted Manuscript published as ERC-21-0179.R1. Accepted for publication: 16 Jul 2021

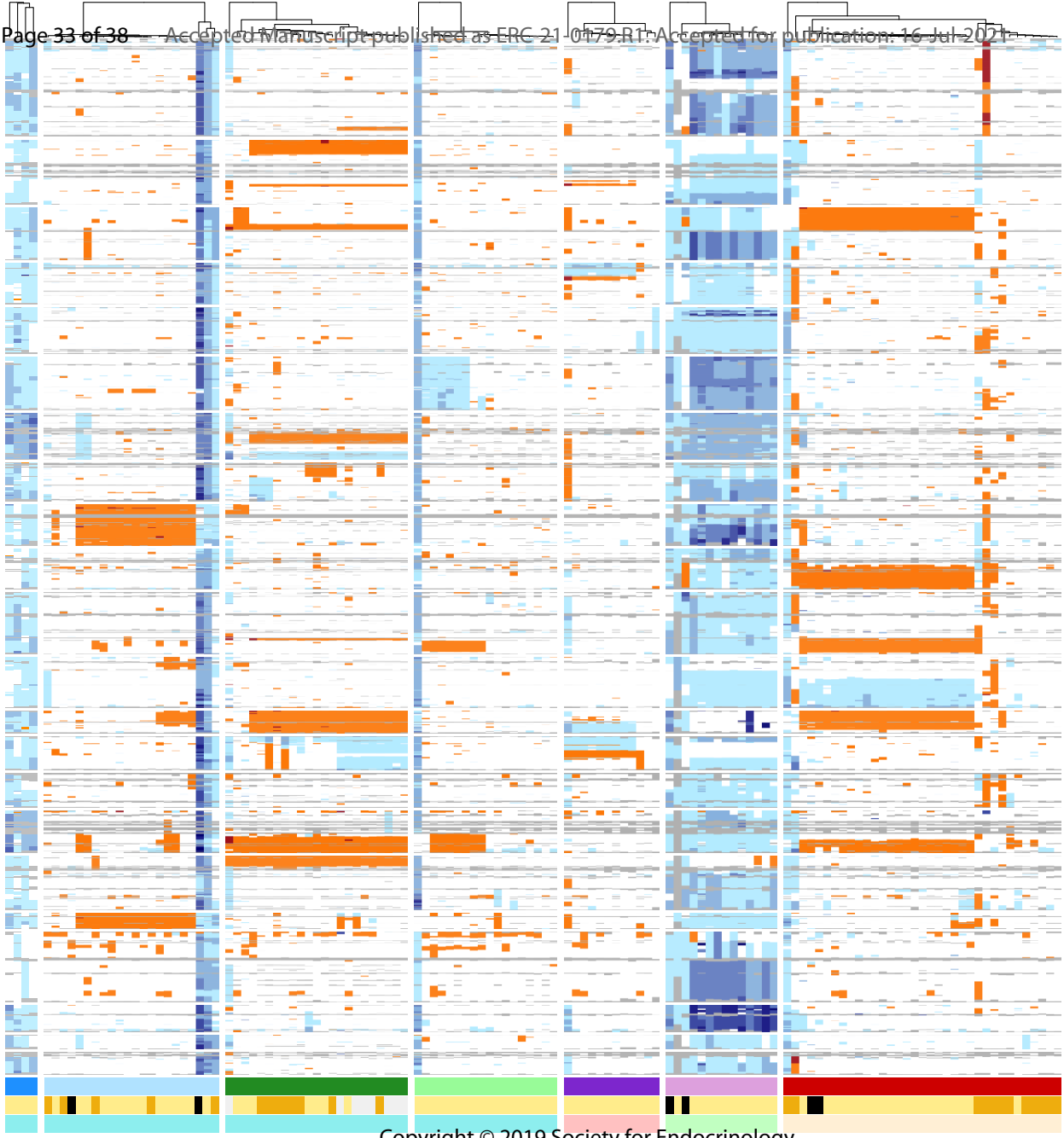

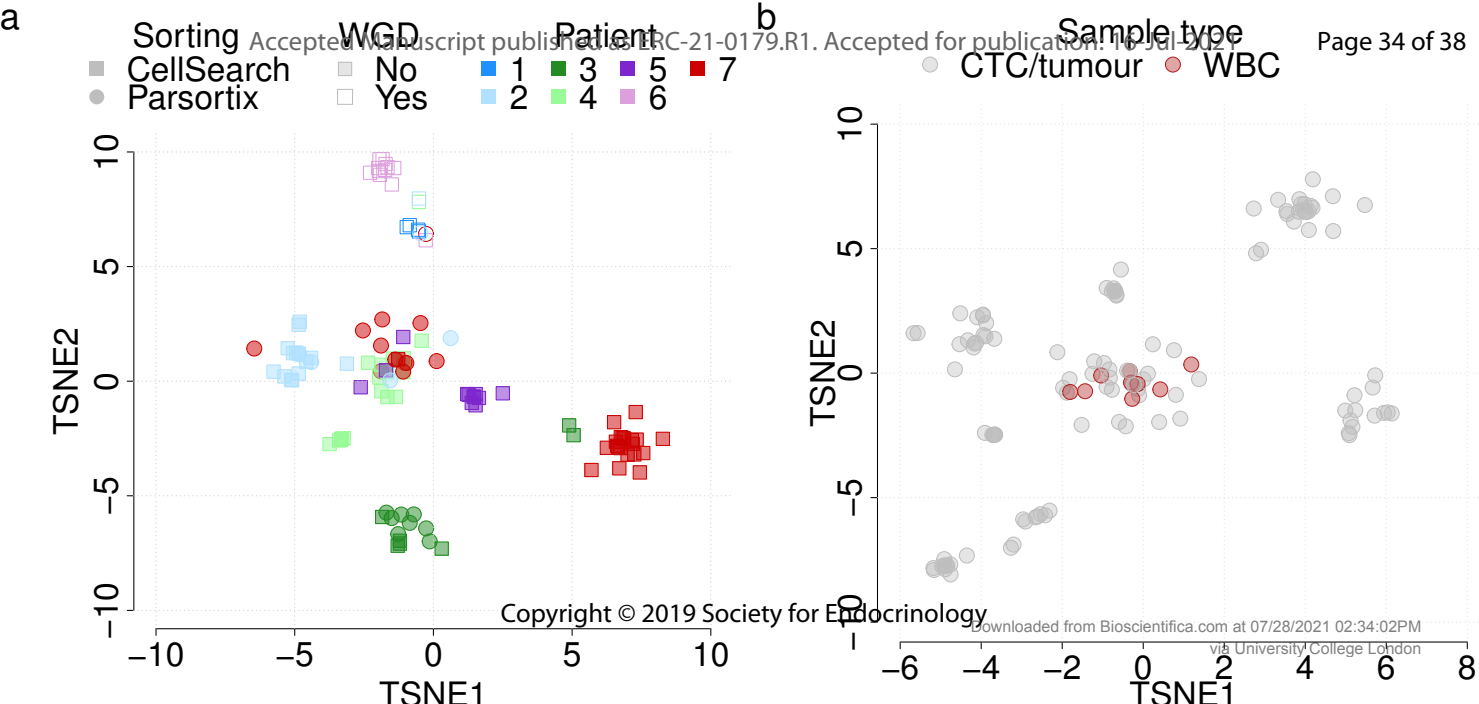

Accepted Manuscript published as ERC-21-0179.R1. Accepted for publication: 16-Jul-2021

a

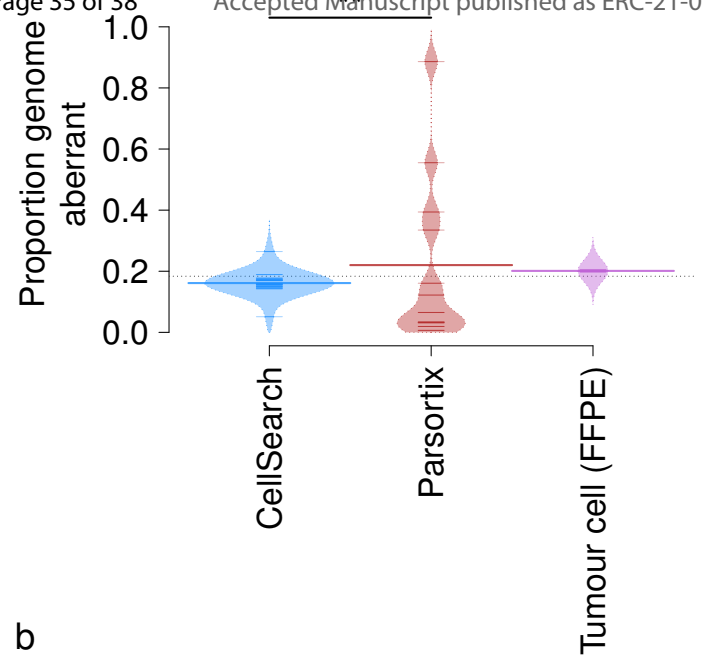

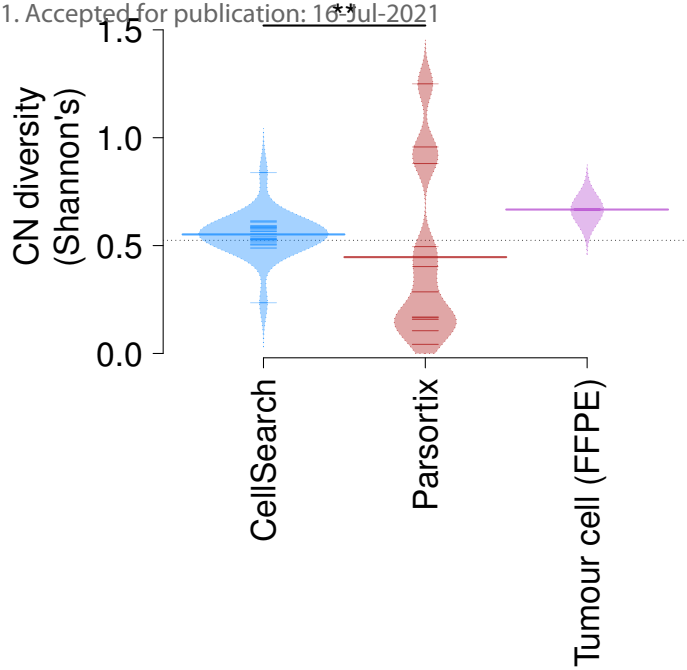

b

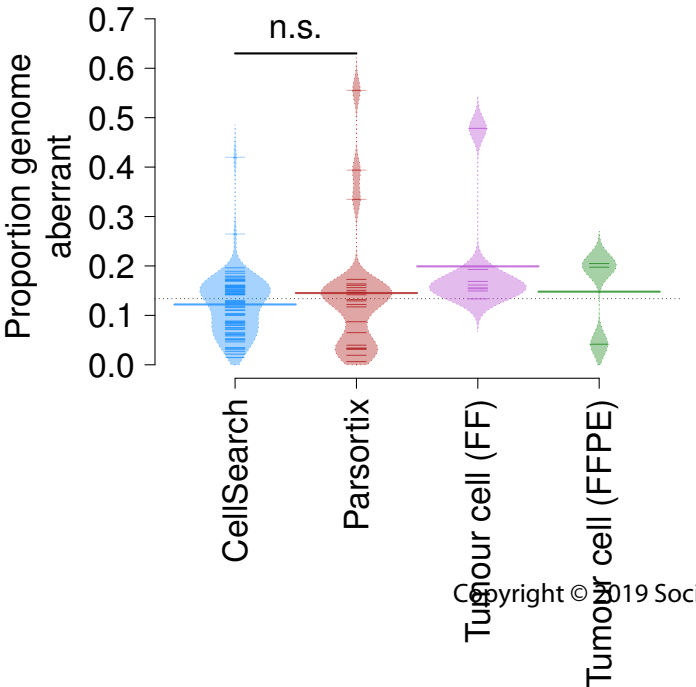

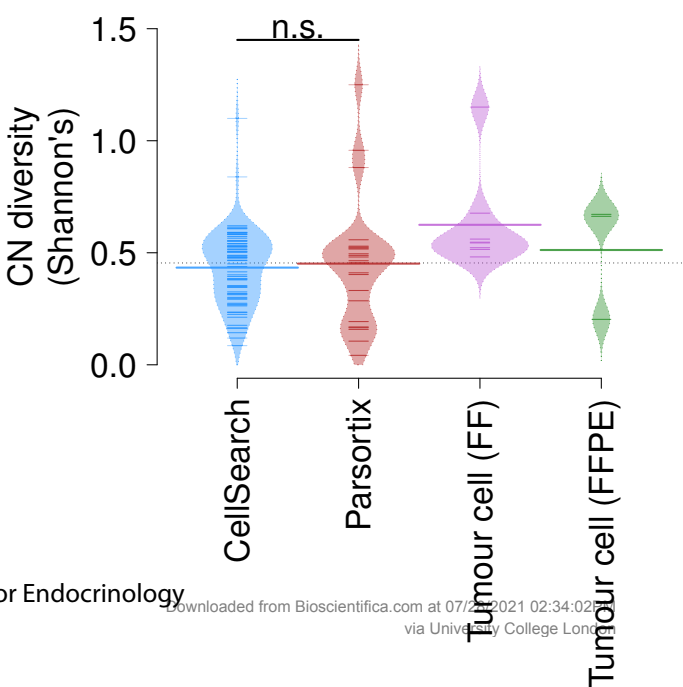

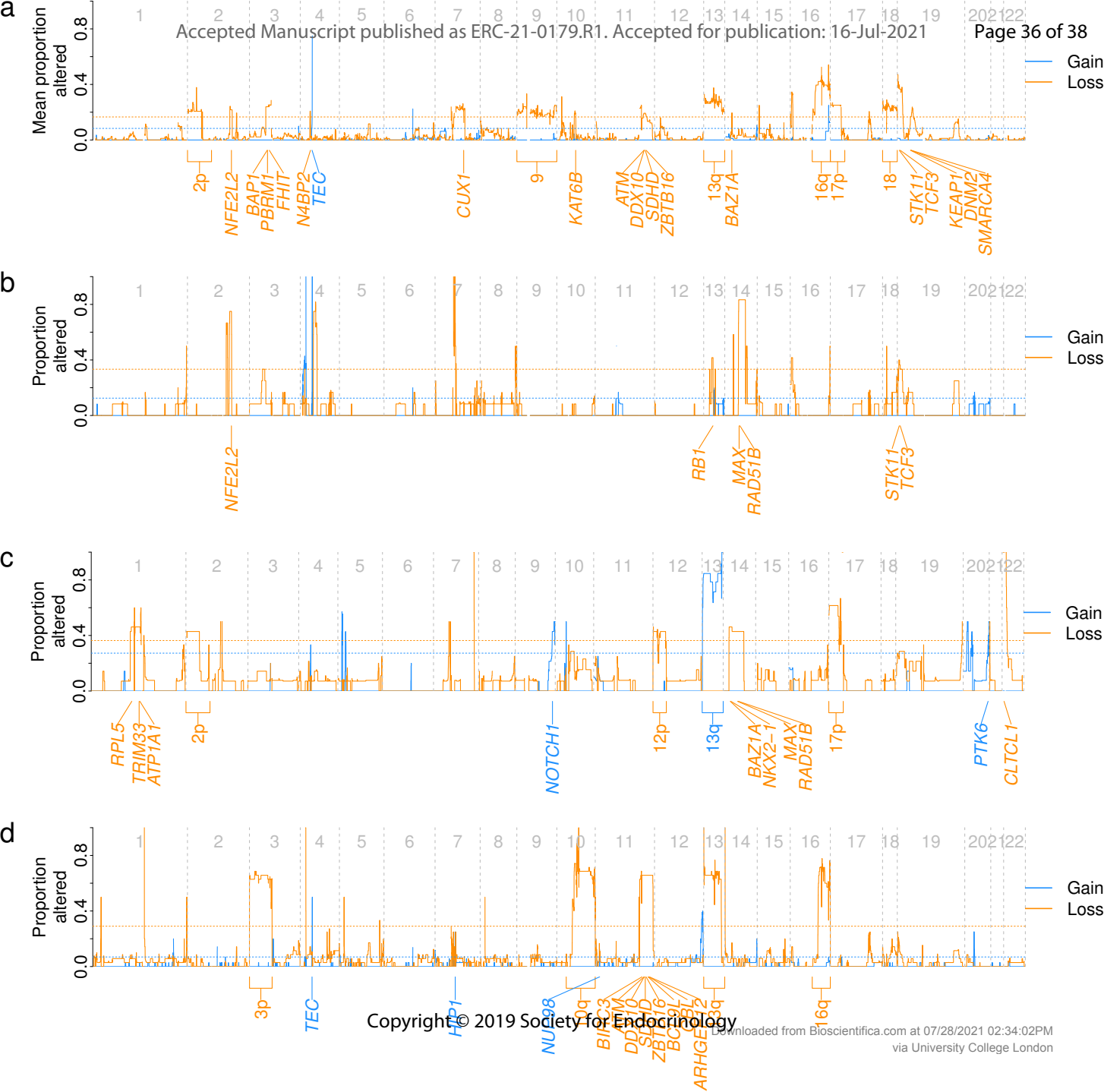

Accepted Manuscript published as ERC-21-0179.R1. Accepted for publication: 16-Jul-2021